hapln1 Defines an Epicardial Cell Subpopulation Required for Cardiomyocyte Expansion During Heart Morphogenesis and Regeneration

Jisheng Sun, *Emory University*
Elizabeth A Peterson, *Emory University*
Annabel Z Wang, *Duke University*
Jianhong Ou, *Duke University*
Kieko E Smith, *Emory University*
Kenneth D Poss, *Duke University*
Jinhu Wang, *Emory University*

Journal Title: CIRCULATION

Volume: Volume 146, Number 1

Publisher: LIPPINCOTT WILLIAMS & WILKINS | 2022-07-05, Pages 48-63

Type of Work: Article | Post-print: After Peer Review

Publisher DOI: 10.1161/CIRCULATIONAHA.121.055468

Permanent URL: https://pid.emory.edu/ark:/25593/w7r46

Final published version:
http://dx.doi.org/10.1161/CIRCULATIONAHA.121.055468

Published in final edited form as:
Circulation. 2022 July 05; 146(1): 48–63. doi:10.1161/CIRCULATIONAHA.121.055468.

hapln1 defines an epicardial cell subpopulation required for cardiomyocyte expansion during heart morphogenesis and regeneration

Jisheng Sun, PhD[1], **Elizabeth A. Peterson, PhD**[1], **Annabel Z. Wang, BA**[2], **Jianhong Ou, PhD**[2], **Kieko E. Smith, BS**[1], **Kenneth D. Poss, PhD**[2,*], **Jinhu Wang, PhD**[1,*]

[1]Division of Cardiology, School of Medicine, Emory University, Atlanta, GA, 30322, USA

[2]Duke Regeneration Center, Department of Cell Biology, Duke University Medical Center, Durham, NC, 27710, USA

Abstract

BACKGROUND: Certain non-mammalian species like zebrafish have an elevated capacity for innate heart regeneration. Understanding how heart regeneration occurs in these contexts can help illuminate cellular and molecular events that can be targets for heart failure prevention or treatment. The epicardium, a mesothelial tissue layer that encompasses the heart, is a dynamic structure that is essential for cardiac regeneration in zebrafish. The extent to which different cell subpopulations or states facilitate heart regeneration requires research attention.

METHODS: To dissect epicardial cell states and associated pro-regenerative functions, we performed single-cell RNA-sequencing and identified 7 epicardial cell clusters in adult zebrafish, 3 of which displayed enhanced cell numbers during regeneration. We identified paralogs of hyaluronan and proteoglycan link protein 1 (*hapln1*) as factors associated with the extracellular matrix (ECM) and largely expressed in cluster 1. We assessed *HAPLN1* expression in published scRNA-seq datasets from different stages and injury states of murine and human hearts, and we performed molecular genetics to determine the requirements for *hapln1*-expressing cells as well as functions of each *hapln1* paralog.

RESULTS: A particular cluster of epicardial cells had the strongest association with regeneration and was marked by expression of *hapln1a* and *hapln1b*. *hapln1* paralogs are expressed in epicardial cells that enclose dedifferentiated and proliferating cardiomyocytes during regeneration. Induced genetic depletion of *hapln1*-expressing cells or genetic inactivation of *hapln1b*

[*]Address for Correspondence: Jinhu Wang, Ph.D., Division of Cardiology, Department of Medicine, Emory University, 315 WMB, 101 Woodruff Circle, Atlanta, Georgia 30322, USA, Phone: (404)-727-9540, jinhu.wang@emory.edu, Kenneth D. Poss, Ph.D., Department of Cell Biology, Duke University Medical Center, 466 Nanaline Duke Building, Box 3709, Durham, NC 27710, USA, Phone: (919)-681-8457, kenneth.poss@duke.edu.

Author contributions: Conceptualization, J.S., K.D.P., and J.W.; methodology, J.S., and J.W.; investigation, J.S., E.A.P., A.Z.W., J.O., K.E.S., and J.W.; formal analysis, J.S., and J.W.; visualization, J.S. and J.W.; writing – original draft, J.W.; writing –review & editing, K.D.P. and J.W.; funding acquisition, K.D.P. and J.W.; supervision, K.D.P. and J.W.. All authors commented on the manuscript.

DECLARATION OF INTERESTS

The authors declare no competing financial interests.

SUMMPLEMENTAL MATERIALS

Expanded Methods

Figure S1–S9

altered deposition of the key ECM component hyaluronic acid (HA), disrupted cardiomyocyte proliferation, and inhibited heart regeneration. We also found that *hapln1*-expressing epicardial cells first emerge at the juvenile stage, when they associate with and are required for focused cardiomyocyte expansion events that direct maturation of the ventricular wall.

CONCLUSIONS: Our findings identify a subset of epicardial cells that emerges in post-embryonic zebrafish and sponsors regions of active cardiomyogenesis during cardiac growth and regeneration. We provide evidence that, as the heart achieves its mature structure, these cells facilitate HA deposition to support formation of the compact muscle layer of the ventricle. They are also required, along with the function of *hapln1b* paralog, in production and organization of HA-containing matrix in cardiac injury sites, enabling normal cardiomyocyte proliferation and muscle regeneration.

Keywords

Zebrafish; Heart; Regeneration; Cardiomyocyte; Epicardium; Extracellular matrix; Hapln1; Hyaluronic acid

INTRODUCTION

Heart failure is a severe, disabling, and costly human condition of insufficient cardiac output to meet the body's demands for oxygen and blood. The primary risk factors contributing to heart failure are coronary artery disease, high blood pressure, and previous myocardial infarction events, all of which coincide with significant cardiac muscle loss and fibrosis[1]. Although the damaged adult mammalian heart has minimal capacity to restore lost cardiac muscle, mammals display measurable regeneration at early neonatal stages, and human studies suggest a low turnover rate in cardiomyocytes (CMs) throughout an individual's lifetime[2, 3, 4, 5]. Thus, a prevailing view is that the adult mammalian heart has endogenous regeneration capabilities but cannot initiate or complete this process after injury.

Zebrafish have exceptionally high cardiac regenerative capacity, based on the ability of adult zebrafish CMs to dedifferentiate and proliferate after major injury[6–10]. While many studies have explored the cell-intrinsic basis of the competency for CM division upon injury during zebrafish heart regeneration[7, 8, 11, 12], other reports have highlighted the essential role of non-myocardial cells, including epicardial, vascular, lymphatic, and neural cells[13–16]. The epicardium is a mesothelial tissue that envelops the cardiac outer surface and is rapidly activated to proliferate, migrate, and cover injuries[17–23], and genetic depletion of the epicardium blocks zebrafish heart regeneration[24]. Conversely, manipulations of the epicardium have been reported to enhance mammalian heart repair[24–28]. As the epicardium is a heterogeneous structure, its cellular constituents require further exploration, especially as to how they might support customized roles during cardiac regeneration.

Here, we applied single-cell RNA-sequencing (scRNA-seq) analysis in zebrafish to examine epicardial subpopulations and how they might contribute to myocardial growth and regeneration. Our studies identify a requirement for a large, regeneration-associated cluster of cells expressing genes encoding the hyaluronic acid (HA)-organizing factors *hapln1a* and *hapln1b*. We find that these cells envelop proliferative CMs during key cardiogenic events

during both heart morphogenesis and regeneration, when they are required for normal HA organization and cardiac muscularization.

METHODS

Data Availability

The authors declare that all data that support the findings of this study are available within the article and its Supplemental Material. The data, analytic methods, and study materials will be available to other researchers for purposes of reproducing the results or replicating the procedure. The scRNA-seq dataset has been submitted to Gene Expression Omnibus (GEO) and the accession number is GSE172511.

Zebrafish and heart injuries

Outbred EK or EK/AB zebrafish 4–10 months old were used for ventricular resection[6] and cardiomyocyte (CM) ablation[8]. For depletion of *hapln1a*:mCherry-NTR-expressing cells, zebrafish were used at 5–12 weeks (juvenile) and 4–12 months (adult). Animal density was maintained at ~4 fish/L in all experiments. To deplete *hapln1a*+ cells, *hapln1a:mCherry-NTR* animals and control siblings were treated with vehicle or 10 mM metronidazole (Mtz) in a 1.5 L mating tank for 14 hours/day over 2 (juvenile) or 3 (adult) days. Transgenic strains described elsewhere were *gata4:EGFP*[29], Z-CAT and *tcf21:nucEGFP*[8], and *tcf21:mCherry-NTR*[24]. Newly constructed strains are described in Supplement Methods. All transgenic strains were analyzed as hemizygotes. All animal procedures were performed in accordance with Emory University and Duke University guidelines.

Histological methods

Histological analyses were performed on 10 μm cryosections of paraformaldehyde-fixed hearts. Primary antibodies used here include: anti-Mef2 (rabbit; Santa Cruz Biotechnology), anti-MF20 (mouse; Developmental Studies Hybridoma Bank), anti-Lcp1 (rabbit, GeneTex), and anti-PCNA (mouse; Sigma). Alexa Fluor secondary antibodies (Invitrogen) used here were: 488 (goat anti-rabbit), 594 (goat anti-rabbit and goat anti-mouse), and 633 (goat anti-mouse).

CM proliferation cycling were quantified as previously described[24] and MF20 staining of 30 dpa hearts for muscularization was performed as previously described[11]. Quantification of *gata4*:EGFP+ expression in adult fish were performed as described[7]. To quantify *gata4*:EGFP$^+$ cell growth, 3 fields of EGFP$^+$ cells in each heart were observed and followed for two days. Images were captured using a stereomicroscope. The extent of EGFP$^+$ growth was determined in pixels by ImageJ software.

To quantify *hapln1b*:EGFP and *hapln1a*:mCherry-NTR colocalization in uninjured and regenerating ventricles, whole-mounted specimens were selected from each group and imaged. Images of ventricles were captured using a 20x objective lens (1,024 × 1,024 pixels). The colocalization between EGFP$^+$ and mCherry$^+$ signals was determined in pixels using JACoP from ImageJ software.

To calculate HA signals, ventricular sections were stained with biotinylated-HABP[30] and fluorescently labeled streptavidin-Alexa-647 conjugate. For adults, images of the ventricle were captured using a 20x objective lens (1,024 × 1,024 pixels), while images of single optical slices of ventricles were acquired using a 63x objective lens (1,024 × 1,024 pixels) in the same position of each ventricle for juveniles. The HA signals were measured in pixels by ImageJ software for signals in the edge of the injury site (163 × 163 μm) of each ventricle. As the number of HA aggregates indicates HA instability, we calculated HA aggregates by the amount of HA dots per unit area of HA signals to determine the HA stability.

To quantify compact muscle thickness, 3 medial, longitudinal sections were selected from each heart and imaged. Single optical slices of the ventricle were acquired using a 63x objective lens (1,024 × 1,024 pixels) in the same position of each ventricle, from sections stained with MF20 antibody. Compact muscle thickness was measured in pixels by ImageJ software.

Single-cell RNA-sequencing

To prepare epicardial cells for single-cell RNA-sequencing analysis, *tcf21:nucEGFP* and *tcf21:nucEGFP:Z-CAT* (*tcf21:nucEGFP*;*cmlc2:CreER*;*bactin2:loxp-mCherry-STOP-loxp-DTA)* transgenic fish were raised to adulthood. Hearts were collected from *tcf21:nucEGFP;Z-CAT* and *tcf21:nucEGFP* transgenic fish at 7 days post 4-hydroxytamoxifen (4-HT) treatment, and digested with 0.26 U/ml Liberase™ Thermolysin Medium (TM) based on a previously published protocol[31]. Dissociated cells were spun down and live $EGFP^+$ cells sorted by flow cytometry. Isolated cells were sent to Emory Integrated Genomics Core (EIGC) center for 10x single-cell RNA-sequencing. Approximately 6,666 cells were loaded per channel for an expected recovery of 4,000 cells. Single-cell RNA-seq libraries were prepared using the Chromium Single Cell 3' Library & Cell Bead Kit v3.1 (Cat. No. 1000128, 1000127, 120262; 10x Genomics) according to manufacturer's protocol. Libraries were sequenced with an Illumina NextSeq550 using mid output 150-cycle kits according to manufacturer specifications. The newly generated scRNA-seq data were demultiplexed, aligned, and quantified using Cell Ranger Single-Cell Software. Preliminary filtered data generated from Cell Ranger were used for downstream analysis by Seurat R package according to standard workflow.

STATISTICAL ANALYSIS

All data are presented as mean ± SEM. All statistical analyses were performed using Prism 7 software (GraphPad). The Mann-Whitney Rank Sum test was used for assessing statistical differences between 2 groups. The Kruskal-Wallis test was performed for 3 group comparisons. The Chi-squared test was used for categorical variables. The results with P values <0.05 were considered statistically significant.

RESULTS

Identification of epicardial cell states during heart regeneration

To identify epicardial subpopulations as defined by gene expression states, we performed single-cell RNA-sequencing (scRNA-seq) analysis using dissociated epicardial cells. Cells

activating the regulatory sequences of the pan epicardial maker *tcf21* were purified from hearts of uninjured *tcf21:nEGFP* animals[8] or those regenerating after induced genetic ablation of ~50% of cardiomyocytes (CMs; Fig. 1A). Genetic ablation injuries produce areas of regeneration throughout the ventricle and assist profiling from whole ventricles, whereas partial resection or cryoinjury leaves only a small area of regenerating tissue[8, 32, 33]. We applied stringent quality filtering and discarded a small number of GFP^{-}/*tcf21*$^{-}$ cells and other non-epicardial cell types like erythroid hematopoietic cells (*gata1a*)[34], myeloid or leukocyte hematopoietic cells (*lcp1*)[35], cardiomyocytes (*myl7*)[36] and endothelial cells (*fli1a*)[37]. We obtained high-quality transcriptomes of 3,644 and 4,225 epicardial cells from uninjured and regenerating hearts, respectively (Figure S1). Unsupervised clustering identified 7 epicardial cell clusters, with each cluster possessing distinct gene expression patterns during regeneration (Fig. 1B and 1C, and Figure S2 and S3). Cluster 1 had the largest cell population, expressing an enrichment of genes associated with muscle development, heart regeneration and extracellular matrix (ECM) organization, for instance expressing high levels of *nrg1*, *fstl1a*, *inhbaa*, *col8a1b,* and *has1*[25, 38–41]. Clusters 2, 3, and 6 are three groups of cells that express genes implicated in regulating immune responses, such as *ccl25b, c4b, cfd*, and *tnfsf12*[42–45]. These clusters had a high degree of overlap, and it is unclear if they represent distinct cellular identities or different stages of epicardial cells. However, we observed a notable difference in cluster 3 with high levels of *crabp1a* and *Frzb*[46, 47], implicated in negative regulation of the retinoic acid and Wnt signaling pathways, respectively. Cluster 4 cells displayed notable expression of cell cycle genes such as *mki67, fen1, mcm2, PCNA*, and *rpa2*[48–52], indicative of a proliferative state. Cluster 5 expressed genes like *dhx58, mxb, rsad2,* and *saa*[53–56], indicative of a defense response. *cxcl12b* expression in cluster 7 suggested responses to chemokines in these cells[57]. Among the identified clusters, clusters 1, 4, and 5 increased in representation during regeneration, with the others decreasing (Fig. 1D). These increased clusters acquire shared functional characteristics during regeneration; for example, they are each associated with the gene ontology (GO) terms tissue regeneration and ECM organization, and clusters 1 and 5 are linked to muscle structure development and angiogenesis (Fig. 1E).

To better define relationships between the epicardial clusters, we performed RNA velocity analysis[58], which infers the direction and rate of cellular state changes based on the relative abundance of spliced and unspliced transcripts. RNA velocity analysis indicated a dynamic movement among all clusters of epicardial cells (Figure S4). We observed a predicted transition from cluster 2 to cluster 1 in both uninjured and regenerating hearts, suggesting that cluster 1 cells originate from cluster 2. Interestingly, there is a predicted transition from cluster 1 to cluster 4 in regenerating hearts, suggesting that proliferating epicardial cells originate from cluster 1 cells.

hapln1a labels epicardial cells that associate with regenerating cardiomyocytes

As cluster 1 was the most heavily represented of the 3 enhanced cell states and enriched with genes related to injury-induced heart regeneration (Fig. 1D and 1E), we focused attention here. Previous studies revealed extracellular matrix (ECM) regulation as a key function of epicardial cells during regeneration, through dynamic production of critical components like fibronectin and connective tissue growth factor[59, 60]. Among the enriched

genes with ECM function were *fstl1a*, *col8a1b, has1,* and *hapln1a*[39, 40] (Figure S2 and S3). In particular, we noted 33% of *tcf21*+ cells express *hapln1a* in uninjured hearts, with an increase to 49.3% in regenerating hearts (Fig. 1F). *hapln1a* encodes an ECM component that belongs to the hyaluronic acid superfamily and stabilizes hyaluronan-proteoglycan complexes[61, 62]. Previous reports indicated that *hapln1a* regulates heart development in zebrafish by instructing areas of ECM expansion, and that *HAPLN1* is required for cardiac wall morphogenesis in mice[63,64]. For additional context, we re-analyzed published scRNA-seq datasets from samples of human and mouse hearts[65–68]. There exists a relative abundance of *HAPLN1*-expressing cells in embryonic human and mouse hearts (Fig. 2A and 2B), with expression observed in fibroblasts and endothelial cells in human and mouse hearts and in mouse CMs (Fig. 2C and 2D), by comparison with adult hearts from these species which have few cells with detectable *HAPLN1* expression (Fig. 2E and 2F). In damaged human and mouse hearts, there is a small increase in the number of cells expressing *HAPLN1*, but this representation is much lower than in embryonic human and mouse hearts (Fig. 2G–2J). These findings indicate that the cellular representation of *HAPLN1* (*hapln1*) expression differs after cardiac injury between species with disparate regenerative capacities.

To visualize *hapln1a* expression, we conducted *in situ* hybridization in adult zebrafish hearts, observing localized signals in the ventricular wall consistent with epicardial tissue (Fig. 3A). To better assess areas of expression, we also generated *hapln1a:EGFP* and *hapln1a:mCherry-NTR* BAC transgenic animals containing sequences 194 kb upstream of the *hapln1a* translation initiation codon and 13 kb downstream of the stop codon. We observed prominent fluorescence signals in the ventricular wall and bulbus arteriosus, with no detectable cardiac expression elsewhere (Fig. 3B, and Figure S5), mimicking endogenous *hapln1a* mRNA expression. *hapln1a*:EGFP$^+$ cells (occasionally referred to for brevity as *hapln1a*$^+$ or *hapln1a*-expressing cells) increased in number during regeneration after genetic myocardial ablation, consistent with our observations from scRNA-seq analysis of *tcf21*$^+$ cells (Figure S5). As predicted by scRNA-seq, *hapln1a*-directed expression occupied a subset of cells marked by transgenic *tcf21*:mCherry fluorescence in uninjured hearts[69] (Fig. 3C), indicating that *hapln1a*$^+$ cells are epicardial or epicardial-derived cells. *hapln1a*-directed fluorescence signals did not colocalize with reporter transgenes marking endothelial or myocardial cells[7, 70] (Fig. 3D and 3E). *hapln1a*:EGFP was not present in the extreme surface layer of epicardium positive for Raldh2 in uninjured hearts[7], whereas cells expressing both of these markers emerged upon injury (Figure S5).

To assess the distribution of *hapln1a*$^+$ cells during regeneration, we examined *hapln1a:EGFP* hearts at various timepoints after partial resection of the ventricular apex. *hapln1a*-expressing cells accumulated adjacent to injuries by 7 days post resection (dpa), and they remained in the wounds and regenerating muscle at 14 and 30 dpa (Fig. 3F). We noticed that 21.23% of *tcf21*$^+$ cells express *hapln1a* in the injury site by 7 dpa, suggesting *hapln1a*$^+$ cells represent a minority of *tcf21*$^+$ cells in the regenerating area after resection surgery (Fig. 3G). Activation of regulatory sequences of the cardiogenic transcription factor *gata4* expression is induced in regenerating CMs and considered a marker of dedifferentiation[7]. We observed *hapln1a*$^+$ cells surrounding dedifferentiated and proliferating *gata4*:EGFP$^+$

CMs during regeneration (Fig. 3H–3J, and Figure S5), suggesting that they may function in muscle regeneration.

Genetic depletion of *hapln1*$^{+}$ cells inhibits cardiac muscle regeneration

To test the requirement for *hapln1a*-expressing cells during heart regeneration, we employed the bacterial nitroreductase (NTR) system for inducible tissue ablation[71]. We generated a new transgenic line and incubated otherwise uninjured *hapln1a:mCherry-NTR* adults with the pro-drug metronidazole (Mtz). This treatment depleted ~97% of ventricular *hapln1a*+ cells, without apparent effects on animal survival or CM proliferation (Figure S6). We then incubated adult *hapln1a:mCherry-NTR* fish and control siblings for 3 days with Mtz at 2 days after resection of the ventricular apex, and collected hearts at various timepoints post-injury.

At 7 dpa, a timepoint at which many CMs in the injury site proliferate, hearts with ablated *hapln1a*$^{+}$ cells displayed a 39% reduction in the percentage of cycling CMs compared to control siblings (Fig. 4A and B). To assess effects on regenerating cardiomyocytes, we imaged and quantified *gata4*:EGFP signals in 14 dpa injury sites (Fig. 4C and D). Mtz-treated *hapln1a:mCherry-NTR* animals displayed a 57% reduction in *gata4*:EGFP tissue on average when compared to controls. By 30 dpa, most *hapln1a:mCherry-NTR* fish exhibited large gaps in the myocardial wall indicative of defective regeneration (Fig. 4E and F). These results indicate that cardiac muscle regeneration requires the presence of the *hapln1a*-expressing epicardial cell population.

hapln1b, but not *hapln1a*, is required for heart regeneration

Analysis of our scRNA-seq dataset indicated that *hapln1a*-expressing epicardial clusters also express *hapln1b* (Fig. 5A, and Figure S7). DNA sequence homology between *hapln1a* and *hapln1b* coding sequences is 69%, and amino acids are 58% identical (Figure S7). Protein homology comparisons between Hapln1a and b revealed the same functional domains. We generated a new *hapln1b:EGFP* BAC reporter strain to visualize *hapln1b*-expressing cells, observing that *hapln1b* signals localized to the epicardium and showed 99% colocalization with *hapln1a*$^{+}$ cells in uninjured ventricles, and 89% colocalization at sites of regeneration (Fig. 5B–5D, and Figure S7). Thus, we postulated that key Hapln1 functions in *hapln1a*-expressing cells could be carried out by Hapln1a, Hapln1b, or both factors.

To determine functions of Hapln1a and Hapln1b during regeneration, we generated large deletions to remove their coding sequences with CRISPR-Cas9 gene-editing. As expected, these mutations disrupted their respective gene products, as determined by Real-time PCR (qPCR) and Western blotting (Figure S7). Similar to alleles generated in a previous study, homozygous *hapln1a* mutant animals showed a transient and minor cardiac dysmorphology at the embryonic stage that did not affect viability[63] (Figure S7). We examined homozygous *hapln1a* and *hapln1b* mutant animals at juvenile and adult stages, and observed similar ventricular morphology of *hapln1a* mutant animals to their wild-type siblings with no obvious difference detected at juvenile and adult stages. Interestingly, *hapln1b* mutant animals show measurably thinner ventricular walls compared with their wild-type siblings at

the juvenile stage. Adult *hapln1b* mutant animals and their siblings have similar ventricular wall morphology (Figure S7).

While *hapln1a* mutant animals trended toward a lower regeneration index score at 30 dpa, most were able to renew a contiguous wall of heart muscle (Fig. 5E and 5F, and Figure S7). These results indicate that *hapln1a* is largely dispensable for heart regeneration. However, in contrast with *hapln1a* mutants, we observed consistently disrupted restoration of the myocardial wall in *hapln1b* mutants at 30 dpa. This phenotype was still evident by 60 dpa (Fig. 5G, 5H, and Figure S7). We then assessed whether *hapln1b* mutations are essential for injury-induced proliferation of CMs. There was a 35% decrease in the 7 dpa CM proliferation index in *hapln1b* mutations compared with their wild-type clutchmates (Fig. 5I and 5J). Together, our results reveal that *hapln1a* and *b* expression mark a subset of epicardial cells that are preferentially affiliated with regenerating CMs, and that Hapln1b is essential for normal heart regeneration.

Depletion of *hapln1a*-expressing cells or inactivation of *hapln1b* result in defective HA deposition during cardiac muscle regeneration

To elucidate the mechanism by which *hapln1*-expressing epicardial cells and Hapln1b impact CM proliferation and regeneration, we assessed the levels and distribution of its substrate, hyaluronic acid (HA). HA has been explored as a biomaterial to assist repair after myocardial infarction[72–74]. Moreover, Tsang and colleagues reported its requirement for heart regeneration[41, 75], finding that inhibition of Has enzymes with UDP glucuronic acid blocked epicardial epithelial-mesenchymal transition (EMT) and migration, reducing CM cycling and muscle regeneration. We observed increased HA presence in the injury site using a fluorescent dye as previously reported[30]; additionally, *has1* is present in cluster 1 in regenerating hearts (Fig. 6A). Notably, HA signals were closely associated with *hapln1a*:EGFP$^+$ cells within the injury area (Fig. 6B), as well as near regions of proliferating CMs and *gata4*:EGFP$^+$ cells, consistent with our Hapln1 analyses and with a role in muscle regeneration (Fig. 6C).

To test requirements for *hapln1a*$^+$ epicardial cells in regulation of cardiac HA, we examined HA in hearts of *hapln1a:mCherry-NTR* animals after Mtz treatment and ventricular resection (Fig. 6D). Amounts of HA were assessed by quantifying fluorescence intensity, and the size of HA aggregates was estimated by quantifying the area of each focus of HA. We found that 7 dpa injury sites of *hapln1a*$^+$ cell depleted animals displayed ~38% less HA (Fig. 6E), and ~47% smaller puncta, compared with wild-type siblings (Fig. 6F). To test whether one or both of the Hapln1 enzymes are required for HA localization, we examined HA distribution at 7 dpa in each *hapln1* mutant line. HA features in regenerating *hapln1a* mutant ventricles were normal (Fig. 6G–6I). By contrast, *hapln1b* mutants displayed a similar quantified amount of HA in 7 dpa wounds as wild-types (Fig. 6J and 6K), however with 51% smaller aggregates (Fig. 6L). The different effects of the *hapln1a* and *hapln1b* mutants on HA deposition are likely to contribute to why only the *hapln1b* mutants display defects in heart regeneration. Our results indicate a mechanism for Hapln1 function during regeneration, in which HA, deposited and organized by epicardial cells, is important for CM proliferation, dedifferentiation, and regeneration during zebrafish heart regeneration.

Regionally localized *hapln1*-expressing cells support the morphogenesis of the ventricular wall in juvenile animals

Cardiac chambers develop in zebrafish by 24 hours post-fertilization (hpf), and their maturation continues throughout both juvenile and early adult life stages. In juvenile zebrafish ventricles, a small number of *gata4*:EGFP$^+$ CMs initially emerge on the chamber surface at ~5 weeks of age, where they proliferate to form the initial clones of compact muscle. These initial clones gradually expand and converge with others to eventually encapsulate the ventricle and create a contiguous wall of compact muscle that is characteristic of adult hearts[76, 77].

To examine roles for *hapln1a*$^+$ cells in ventricular morphogenesis, we assessed hearts of embryonic and juvenile *hapln1a:EGFP* animals. We initially observed *hapln1a*:EGFP$^+$ signals in CMs by 2 dpf, with no detectable expression in endothelial or epicardial cells. EGFP$^+$ cells were not visible in the embryonic heart at 5 dpf (Figure S8). Interestingly, while *tcf21*$^+$ epicardial cells coat the juvenile ventricle, we found that they do not activate *hapln1a* regulatory sequences until 5 weeks post-fertilization (wpf). Then, a small cluster of *hapln1a*$^+$ cells expressing *tcf21*, but not Raldh2 or CM markers, appears at the ventricular base and gradually expands and spreads over the entire ventricle by 12 wpf (Fig. 7A and Figure S8). To examine a potential association with compact wall formation, we analyzed hearts of *hapln1a:mCherry-NTR*;*gata4:EGFP* fish from 5 to 12 wpf. Imaging of the ventricular surface revealed enclosure of *gata4*:EGFP$^+$ CMs by *hapln1a*$^+$ cells at all timepoints (Fig. 7B and 7C), an observation confirmed by analyses of tissue sections (Fig. 7D). To identify dynamics of HA during heart morphogenesis, we assessed its localization on the ventricular surface in juvenile animals. We found strong concordance of HA signals with both *hapln1a*:EGFP$^+$ epicardial cells and *gata4*:EGFP+ CMs (Fig. 7E and 7F), suggesting a similar role for Hapln1 factors in organizing HA as during regeneration.

To test requirements of *hapln1a*$^+$ cells in genesis of the compact myocardium, we ablated *hapln1a*$^+$ cells at 6–7 weeks post fertilization. Juvenile *hapln1a:mCherry-NTR; gata4:EGFP* animals and *gata4:EGFP* siblings were treated with Mtz, and their hearts were collected for histological analysis at 10 and 30 days post-treatment (dpt). HA amounts in the ventricular wall were reduced by ~53% compared with wild-type siblings at 3 dpt (Fig. 8A and 8B). We found that *hapln1a*+ cell-depleted hearts displayed 35% lower *gata4*:EGFP fluorescence density when compared with control siblings at 10 dpt (Fig. 8C and 8D). At 30 dpt, fish with a depleted *hapln1a*$^+$ cell population showed a normal overall cardiac shape but disorganized compact muscle, with gaps in the ventricular wall and a 52% reduction in the thickness of the compact layer (Fig. 8E and 8F, and Figure S9). By 60 dpt, these animals still displayed a 32% reduction in compact layer thickness (Figure S9). We also assessed *gata4*:EGFP$^+$ CMs after depleting *hapln1a*$^+$ cells in juvenile hearts in an *ex vivo* setting that enables survival of beating hearts in tissue culture for several weeks[24]. Whereas *gata4*:EGFP$^+$ CMs expanded on the ventricular surface in the presence of the full complement of *hapln1a*-positive tissue, such growth rarely occurred in *hapln1a:mCherry-NTR* ventricles, with *gata4*:EGFP$^+$ CM expansion reduced by ~90% compared with controls (Fig. 8G and 8H).

In total, our observations reveal a *hapln1a*-expressing epicardial cell subpopulation that emerges at the juvenile stage and is necessary for key sites of localized cardiomyogenic

activity. By controlling the ECM microenvironment, these cells contribute to compact muscle growth that completes, and later helps regenerate, the layering of the zebrafish ventricle.

DISCUSSION

Here we describe cellular heterogeneity in the epicardium of adult zebrafish, including the appearance of 3 cellular states associated with heart regeneration. Several recent studies using single-cell technologies have revealed the presence of cells or cell states that are preferential to a regeneration context, including skeletal progenitors in axolotl limbs, planarian stem cells, mammalian CMs from different life stages, murine hair follicle stem cells and hepatic cells[78–82]. Although the epicardium is established by the fourth day of life in zebrafish, we report here a latent subpopulation of epicardial cells that emerges coincident with compact muscle in 5-week-old juvenile animals. Our results indicate a key function of *hapln1a*-expressing cells is to oversee principal cardiogenic activities of compact muscle. These include its initial emergence and maintenance as muscle clones on the ventricular surface, and during CM proliferation to replace wall areas lost after a massive injury.

Epicardial cells are known to secrete developmental factors, including many ECM components, during heart regeneration[25, 83], ostensibly as a process of building a nurturing scaffold. Hapln1 enzymes are responsible for the processing and organization of HA within the ECM, which has been recently implicated in heart regeneration. HA and its derivatives are biodegradable; biocompatible; promote faster healing of injured tissues; and support cells in relevant processes including survival, proliferation, and differentiation. Injectable HA-based therapies for cardiovascular disease are rapidly gaining attention because of the benefits obtained in preclinical models of myocardial infarction. HA-based hydrogels, especially as a vehicle for stem cells, have been associated with improvements to the process of cardiac repair by stimulating angiogenesis, reducing inflammation, and supporting local and grafted cells in their reparative functions[75]. We find tight associations of HA deposition during regeneration both with *hapln1* gene expression itself, as well as with CM proliferation and the *gata4*:EGFP indicator of dedifferentiation. Moreover, HA deposition is altered in certain manipulations of *hapln1* genes or *hapln1a*-expressing cells. Thus, we infer that HA organization in cardiac injuries is the key mechanism by which the expression of *hapln1* genes in epicardial cells influences cardiomyogenesis. While our initial investigations focused on the *hapln1a* gene, our genetic manipulations indicate that the *hapln1a* gene product is dispensable for HA organization and indicators of regeneration, whereas *hapln1b* is required for these events. There are many potential reasons for this, including genetic compensation, differential post-translational modifications, differential *in vivo* activity, and differential interactors. Understanding the developmental timing of the appearance of *hapln1*-expressing epicardial cells and how they control foci of cardiogenesis can inspire new ideas for targeted tissue regeneration.

Supplementary Material

Refer to Web version on PubMed Central for supplementary material.

ACKNOWLEDGMENTS

We thank Weilan Lin for zebrafish care and the Developmental Studies Hybridoma Bank for antibodies. Microscopy data for this study were acquired and analyzed through the use of the Microscopy in Medicine Core in Cardiology at Emory. The scRNA-seq was supported by the Woodruff Health Sciences Center (WHSC)'s 10X Single Cell Sequencing Seed Grant to J.W.

FUNDING SOURCES

This work was supported by a NIH T32 training fellowship (5T32HL007745–28) to E.A.P.; grants from American Heart Association (AHA) (16MERIT27940012) and NHLBI (R35 HL150713) to K.D.P.; and grants from NHLBI (R56HL142762, R01HL142762) to J.W. The Microscopy in Medicine Core in Cardiology at Emory was supported by NIH grant (P01 HL095070).

Non-standard Abbreviations and Acronyms

Hapln1	hyaluronan and proteoglycan link protein 1
HA	hyaluronic acid
Mtz	metronidazole
NTR	nitroreductase
Mef2	myocyte enhancer factor-2

REFERENCES

1. McMurray JJ. Clinical practice. Systolic heart failure. N Engl J Med. 2010;362:228–38. [PubMed: 20089973]
2. Bersell K, Arab S, Haring B and Kuhn B. Neuregulin1/ErbB4 signaling induces cardiomyocyte proliferation and repair of heart injury. Cell. 2009;138:257–70. [PubMed: 19632177]
3. Senyo SE, Steinhauser ML, Pizzimenti CL, Yang VK, Cai L, Wang M, Wu TD, Guerquin-Kern JL, Lechene CP and Lee RT. Mammalian heart renewal by pre-existing cardiomyocytes. Nature. 2013;493:433–6. [PubMed: 23222518]
4. Porrello ER, Mahmoud AI, Simpson E, Hill JA, Richardson JA, Olson EN and Sadek HA. Transient regenerative potential of the neonatal mouse heart. Science. 2011;331:1078–80. [PubMed: 21350179]
5. Bergmann O, Bhardwaj RD, Bernard S, Zdunek S, Barnabe-Heider F, Walsh S, Zupicich J, Alkass K, Buchholz BA, Druid H, et al. Evidence for cardiomyocyte renewal in humans. Science. 2009;324:98–102. [PubMed: 19342590]
6. Poss KD, Wilson LG and Keating MT. Heart regeneration in zebrafish. Science. 2002;298:2188–90. [PubMed: 12481136]
7. Kikuchi K, Holdway JE, Werdich AA, Anderson RM, Fang Y, Egnaczyk GF, Evans T, Macrae CA, Stainier DY and Poss KD. Primary contribution to zebrafish heart regeneration by gata4(+) cardiomyocytes. Nature. 2010;464:601–5. [PubMed: 20336144]
8. Wang J, Panakova D, Kikuchi K, Holdway JE, Gemberling M, Burris JS, Singh SP, Dickson AL, Lin YF, Sabeh MK, et al. The regenerative capacity of zebrafish reverses cardiac failure caused by genetic cardiomyocyte depletion. Development. 2011;138:3421–30. [PubMed: 21752928]
9. Gonzalez-Rosa JM, Martin V, Peralta M, Torres M and Mercader N. Extensive scar formation and regression during heart regeneration after cryoinjury in zebrafish. Development. 2011;138:1663–74. [PubMed: 21429987]
10. Chablais F, Veit J, Rainer G and Jazwinska A. The zebrafish heart regenerates after cryoinjury-induced myocardial infarction. BMC Dev Biol. 2011;11:21. [PubMed: 21473762]

11. Jopling C, Sleep E, Raya M, Marti M, Raya A and Izpisua Belmonte JC. Zebrafish heart regeneration occurs by cardiomyocyte dedifferentiation and proliferation. Nature. 2010;464:606–9. [PubMed: 20336145]
12. Gonzalez-Rosa JM, Sharpe M, Field D, Soonpaa MH, Field LJ, Burns CE and Burns CG. Myocardial Polyploidization Creates a Barrier to Heart Regeneration in Zebrafish. Dev Cell. 2018;44:433–446 e7. [PubMed: 29486195]
13. Marin-Juez R, Marass M, Gauvrit S, Rossi A, Lai SL, Materna SC, Black BL and Stainier DY. Fast revascularization of the injured area is essential to support zebrafish heart regeneration. Proc Natl Acad Sci U S A. 2016;113:11237–11242. [PubMed: 27647901]
14. Harrison MR, Feng X, Mo G, Aguayo A, Villafuerte J, Yoshida T, Pearson CA, Schulte-Merker S and Lien CL. Late developing cardiac lymphatic vasculature supports adult zebrafish heart function and regeneration. Elife. 2019;8.
15. Gancz D, Perlmoter G and Yaniv K. Formation and Growth of Cardiac Lymphatics during Embryonic Development, Heart Regeneration, and Disease. Cold Spring Harb Perspect Biol. 2020;12.
16. Mahmoud AI, O'Meara CC, Gemberling M, Zhao L, Bryant DM, Zheng R, Gannon JB, Cai L, Choi WY, et al. Nerves Regulate Cardiomyocyte Proliferation and Heart Regeneration. Dev Cell. 2015;34:387–99. [PubMed: 26256209]
17. Lepilina A, Coon AN, Kikuchi K, Holdway JE, Roberts RW, Burns CG and Poss KD. A dynamic epicardial injury response supports progenitor cell activity during zebrafish heart regeneration. Cell. 2006;127:607–19. [PubMed: 17081981]
18. Kim J, Wu Q, Zhang Y, Wiens KM, Huang Y, Rubin N, Shimada H, Handin RI, Chao MY, Tuan TL, Starnes VA and Lien CL. PDGF signaling is required for epicardial function and blood vessel formation in regenerating zebrafish hearts. Proc Natl Acad Sci U S A. 2010;107:17206–10. [PubMed: 20858732]
19. Cao J and Poss KD. The epicardium as a hub for heart regeneration. Nat Rev Cardiol. 2018.
20. Quijada P, Trembley MA and Small EM. The Role of the Epicardium During Heart Development and Repair. Circ Res. 2020;126:377–394. [PubMed: 31999538]
21. Weinberger M, Simoes FC, Patient R, Sauka-Spengler T and Riley PR. Functional Heterogeneity within the Developing Zebrafish Epicardium. Dev Cell. 2020;52:574–590 e6. [PubMed: 32084358]
22. Simoes FC and Riley PR. The ontogeny, activation and function of the epicardium during heart development and regeneration. Development. 2018;145.
23. Gonzalez-Rosa JM, Peralta M and Mercader N. Pan-epicardial lineage tracing reveals that epicardium derived cells give rise to myofibroblasts and perivascular cells during zebrafish heart regeneration. Dev Biol. 2012;370:173–86. [PubMed: 22877945]
24. Wang J, Cao J, Dickson AL and Poss KD. Epicardial regeneration is guided by cardiac outflow tract and Hedgehog signalling. Nature. 2015;522:226–230. [PubMed: 25938716]
25. Wei K, Serpooshan V, Hurtado C, Diez-Cunado M, Zhao M, Maruyama S, Zhu W, Fajardo G, Noseda M, Nakamura K, et al. Epicardial FSTL1 reconstitution regenerates the adult mammalian heart. Nature. 2015;525:479–85. [PubMed: 26375005]
26. Cao J, Wang J, Jackman CP, Cox AH, Trembley MA, Balowski JJ, Cox BD, De Simone A, Dickson AL, Di Talia S, et al. Tension Creates an Endoreplication Wavefront that Leads Regeneration of Epicardial Tissue. Dev Cell. 2017;42:600–615 e4. [PubMed: 28950101]
27. Huang GN, Thatcher JE, McAnally J, Kong Y, Qi X, Tan W, DiMaio JM, Amatruda JF, Gerard RD, Hill JA, et al. C/EBP transcription factors mediate epicardial activation during heart development and injury. Science. 2012;338:1599–603. [PubMed: 23160954]
28. Kikuchi K, Holdway JE, Major RJ, Blum N, Dahn RD, Begemann G and Poss KD. Retinoic acid production by endocardium and epicardium is an injury response essential for zebrafish heart regeneration. Dev Cell. 2011;20:397–404. [PubMed: 21397850]
29. Heicklen-Klein A and Evans T. T-box binding sites are required for activity of a cardiac GATA-4 enhancer. Developmental biology. 2004;267:490–504. [PubMed: 15013808]
30. Toole BP, Yu Q and Underhill CB. Hyaluronan and hyaluronan-binding proteins. Probes for specific detection. Methods Mol Biol. 2001;171:479–85. [PubMed: 11450261]

31. Spanjaard B, Hu B, Mitic N, Olivares-Chauvet P, Janjuha S, Ninov N and Junker JP. Simultaneous lineage tracing and cell-type identification using CRISPR-Cas9-induced genetic scars. Nat Biotechnol. 2018;36:469–473. [PubMed: 29644996]
32. Karra R, Knecht AK, Kikuchi K and Poss KD. Myocardial NF-kappaB activation is essential for zebrafish heart regeneration. Proc Natl Acad Sci U S A. 2015;112:13255–60. [PubMed: 26472034]
33. Shoffner A, Cigliola V, Lee N, Ou J and Poss KD. Tp53 Suppression Promotes Cardiomyocyte Proliferation during Zebrafish Heart Regeneration. Cell Rep. 2020;32:108089. [PubMed: 32877671]
34. Lyons SE, Lawson ND, Lei L, Bennett PE, Weinstein BM and Liu PP. A nonsense mutation in zebrafish gata1 causes the bloodless phenotype in vlad tepes. Proc Natl Acad Sci U S A. 2002;99:5454–9. [PubMed: 11960002]
35. Kell MJ, Riccio RE, Baumgartner EA, Compton ZJ, Pecorin PJ, Mitchell TA, Topczewski J and LeClair EE. Targeted deletion of the zebrafish actin-bundling protein L-plastin (lcp1). PLoS One. 2018;13:e0190353. [PubMed: 29293625]
36. Huang CJ, Tu CT, Hsiao CD, Hsieh FJ and Tsai HJ. Germ-line transmission of a myocardium-specific GFP transgene reveals critical regulatory elements in the cardiac myosin light chain 2 promoter of zebrafish. Dev Dyn. 2003;228:30–40. [PubMed: 12950077]
37. Harrison MR, Bussmann J, Huang Y, Zhao L, Osorio A, Burns CG, Burns CE, Sucov HM, Siekmann AF and Lien CL. Chemokine-guided angiogenesis directs coronary vasculature formation in zebrafish. Dev Cell. 2015;33:442–54. [PubMed: 26017769]
38. Gemberling M, Karra R, Dickson AL and Poss KD. Nrg1 is an injury-induced cardiomyocyte mitogen for the endogenous heart regeneration program in zebrafish. Elife. 2015;4.
39. Dogra D, Ahuja S, Kim HT, Rasouli SJ, Stainier DYR and Reischauer S. Opposite effects of Activin type 2 receptor ligands on cardiomyocyte proliferation during development and repair. Nat Commun. 2017;8:1902. [PubMed: 29196619]
40. Simoes FC, Cahill TJ, Kenyon A, Gavriouchkina D, Vieira JM, Sun X, Pezzolla D, Ravaud C, Masmanian E, Weinberger M, et al. Macrophages directly contribute collagen to scar formation during zebrafish heart regeneration and mouse heart repair. Nat Commun. 2020;11:600. [PubMed: 32001677]
41. Missinato MA, Tobita K, Romano N, Carroll JA and Tsang M. Extracellular component hyaluronic acid and its receptor Hmmr are required for epicardial EMT during heart regeneration. Cardiovasc Res. 2015;107:487–98. [PubMed: 26156497]
42. Zaballos A, Gutierrez J, Varona R, Ardavin C and Marquez G. Cutting edge: identification of the orphan chemokine receptor GPR-9–6 as CCR9, the receptor for the chemokine TECK. J Immunol. 1999;162:5671–5. [PubMed: 10229797]
43. Noris M and Remuzzi G. Overview of complement activation and regulation. Semin Nephrol. 2013;33:479–92. [PubMed: 24161035]
44. Volanakis JE and Narayana SV. Complement factor D, a novel serine protease. Protein Sci. 1996;5:553–64. [PubMed: 8845746]
45. Winkles JA. The TWEAK-Fn14 cytokine-receptor axis: discovery, biology and therapeutic targeting. Nat Rev Drug Discov. 2008;7:411–25. [PubMed: 18404150]
46. Liu RZ, Garcia E, Glubrecht DD, Poon HY, Mackey JR and Godbout R. CRABP1 is associated with a poor prognosis in breast cancer: adding to the complexity of breast cancer cell response to retinoic acid. Mol Cancer. 2015;14:129. [PubMed: 26142905]
47. Leyns L, Bouwmeester T, Kim SH, Piccolo S and De Robertis EM. Frzb-1 is a secreted antagonist of Wnt signaling expressed in the Spemann organizer. Cell. 1997;88:747–56. [PubMed: 9118218]
48. Scholzen T and Gerdes J. The Ki-67 protein: from the known and the unknown. J Cell Physiol. 2000;182:311–22. [PubMed: 10653597]
49. Warbrick E, Coates PJ and Hall PA. Fen1 expression: a novel marker for cell proliferation. J Pathol. 1998;186:319–24. [PubMed: 10211123]
50. Yousef EM, Furrer D, Laperriere DL, Tahir MR, Mader S, Diorio C and Gaboury LA. MCM2: An alternative to Ki-67 for measuring breast cancer cell proliferation. Mod Pathol. 2017;30:682–697. [PubMed: 28084344]

51. Kelman Z PCNA: structure, functions and interactions. Oncogene. 1997;14:629–40. [PubMed: 9038370]
52. Zou Y, Liu Y, Wu X and Shell SM. Functions of human replication protein A (RPA): from DNA replication to DNA damage and stress responses. J Cell Physiol. 2006;208:267–73. [PubMed: 16523492]
53. Uhlar CM and Whitehead AS. Serum amyloid A, the major vertebrate acute-phase reactant. Eur J Biochem. 1999;265:501–23. [PubMed: 10504381]
54. Saito T, Hirai R, Loo YM, Owen D, Johnson CL, Sinha SC, Akira S, Fujita T and Gale M Jr. Regulation of innate antiviral defenses through a shared repressor domain in RIG-I and LGP2. Proc Natl Acad Sci U S A. 2007;104:582–7. [PubMed: 17190814]
55. Crameri M, Bauer M, Caduff N, Walker R, Steiner F, Franzoso FD, Gujer C, Boucke K, Kucera T, Zbinden A, et al. MxB is an interferon-induced restriction factor of human herpesviruses. Nat Commun. 2018;9:1980. [PubMed: 29773792]
56. Mattijssen S and Pruijn GJ. Viperin, a key player in the antiviral response. Microbes Infect. 2012;14:419–26. [PubMed: 22182524]
57. Janssens R, Struyf S and Proost P. The unique structural and functional features of CXCL12. Cell Mol Immunol. 2018;15:299–311. [PubMed: 29082918]
58. La Manno G, Soldatov R, Zeisel A, Braun E, Hochgerner H, Petukhov V, Lidschreiber K, Kastriti ME, Lonnerberg P, Furlan A, et al. RNA velocity of single cells. Nature. 2018;560:494–498. [PubMed: 30089906]
59. Wang J, Karra R, Dickson AL and Poss KD. Fibronectin is deposited by injury-activated epicardial cells and is necessary for zebrafish heart regeneration. Dev Biol. 2013;382:427–35. [PubMed: 23988577]
60. Mukherjee D, Wagh G, Mokalled MH, Kontarakis Z, Dickson AL, Rayrikar A, Gunther S, Poss KD, Stainier DYR and Patra C. Ccn2a is an injury-induced matricellular factor that promotes cardiac regeneration in zebrafish. Development. 2021;148.
61. Watanabe H and Yamada Y. Mice lacking link protein develop dwarfism and craniofacial abnormalities. Nat Genet. 1999;21:225–9. [PubMed: 9988279]
62. Spicer AP, Joo A and Bowling RA Jr. A hyaluronan binding link protein gene family whose members are physically linked adjacent to chondroitin sulfate proteoglycan core protein genes: the missing links. J Biol Chem. 2003;278:21083–91. [PubMed: 12663660]
63. Derrick CJ, Sanchez-Posada J, Hussein F, Tessadori F, Pollitt EJG, Savage AM, Wilkinson RN, Chico TJ, van Eeden FJ, et al. Asymmetric Hapln1a drives regionalised cardiac ECM expansion and promotes heart morphogenesis in zebrafish development. Cardiovasc Res. 2021.
64. Wirrig EE, Snarr BS, Chintalapudi MR, O'Neal JL, Phelps AL, Barth JL, Fresco VM, Kern CB, Mjaatvedt CH, Toole BP, et al. Cartilage link protein 1 (Crtl1), an extracellular matrix component playing an important role in heart development. Dev Biol. 2007;310:291–303. [PubMed: 17822691]
65. Asp M, Giacomello S, Larsson L, Wu C, Furth D, Qian X, Wardell E, Custodio J, Reimegard J, Salmen F, et al. A Spatiotemporal Organ-Wide Gene Expression and Cell Atlas of the Developing Human Heart. Cell. 2019;179:1647–1660 e19. [PubMed: 31835037]
66. Wang L, Yu P, Zhou B, Song J, Li Z, Zhang M, Guo G, Wang Y, Chen X, et al. Single-cell reconstruction of the adult human heart during heart failure and recovery reveals the cellular landscape underlying cardiac function. Nat Cell Biol. 2020;22:108–119. [PubMed: 31915373]
67. de Soysa TY, Ranade SS, Okawa S, Ravichandran S, Huang Y, Salunga HT, Schricker A, Del Sol A, Gifford CA and Srivastava D. Single-cell analysis of cardiogenesis reveals basis for organ-level developmental defects. Nature. 2019;572:120–124. [PubMed: 31341279]
68. Farbehi N, Patrick R, Dorison A, Xaymardan M, Janbandhu V, Wystub-Lis K, Ho JW, Nordon RE and Harvey RP. Single-cell expression profiling reveals dynamic flux of cardiac stromal, vascular and immune cells in health and injury. Elife. 2019;8.
69. Kikuchi K, Gupta V, Wang J, Holdway JE, Wills AA, Fang Y and Poss KD. tcf21+ epicardial cells adopt non-myocardial fates during zebrafish heart development and regeneration. Development. 2011;138:2895–902. [PubMed: 21653610]

70. Lawson ND and Weinstein BM. In vivo imaging of embryonic vascular development using transgenic zebrafish. Dev Biol. 2002;248:307–18. [PubMed: 12167406]
71. Curado S, Stainier DY and Anderson RM. Nitroreductase-mediated cell/tissue ablation in zebrafish: a spatially and temporally controlled ablation method with applications in developmental and regeneration studies. Nat Protoc. 2008;3:948–54. [PubMed: 18536643]
72. Chi NH, Yang MC, Chung TW, Chen JY, Chou NK and Wang SS. Cardiac repair achieved by bone marrow mesenchymal stem cells/silk fibroin/hyaluronic acid patches in a rat of myocardial infarction model. Biomaterials. 2012;33:5541–51. [PubMed: 22575829]
73. Ifkovits JL, Tous E, Minakawa M, Morita M, Robb JD, Koomalsingh KJ, Gorman JH 3rd, Gorman RC and Burdick JA. Injectable hydrogel properties influence infarct expansion and extent of postinfarction left ventricular remodeling in an ovine model. Proc Natl Acad Sci U S A. 2010;107:11507–12. [PubMed: 20534527]
74. Yoon SJ, Fang YH, Lim CH, Kim BS, Son HS, Park Y and Sun K. Regeneration of ischemic heart using hyaluronic acid-based injectable hydrogel. J Biomed Mater Res B Appl Biomater. 2009;91:163–71. [PubMed: 19399850]
75. Bonafe F, Govoni M, Giordano E, Caldarera CM, Guarnieri C and Muscari C. Hyaluronan and cardiac regeneration. J Biomed Sci. 2014;21:100. [PubMed: 25358954]
76. Gupta V and Poss KD. Clonally dominant cardiomyocytes direct heart morphogenesis. Nature. 2012;484:479–84. [PubMed: 22538609]
77. Gupta V, Gemberling M, Karra R, Rosenfeld GE, Evans T and Poss KD. An injury-responsive gata4 program shapes the zebrafish cardiac ventricle. Curr Biol. 2013;23:1221–7. [PubMed: 23791730]
78. Gerber T, Murawala P, Knapp D, Masselink W, Schuez M, Hermann S, Gac-Santel M, Nowoshilow S, Kageyama J, Khattak S, et al. Single-cell analysis uncovers convergence of cell identities during axolotl limb regeneration. Science. 2018;362.
79. Zeng A, Li H, Guo L, Gao X, McKinney S, Wang Y, Yu Z, Park J, Semerad C, Ross E, et al. Prospectively Isolated Tetraspanin(+) Neoblasts Are Adult Pluripotent Stem Cells Underlying Planaria Regeneration. Cell. 2018;173:1593–1608 e20. [PubMed: 29906446]
80. Cui M, Wang Z, Chen K, Shah AM, Tan W, Duan L, Sanchez-Ortiz E, Li H, Xu L, Liu N, et al. Dynamic Transcriptional Responses to Injury of Regenerative and Non-regenerative Cardiomyocytes Revealed by Single-Nucleus RNA Sequencing. Dev Cell. 2020;55:665–667. [PubMed: 33290696]
81. Yang H, Adam RC, Ge Y, Hua ZL and Fuchs E. Epithelial-Mesenchymal Micro-niches Govern Stem Cell Lineage Choices. Cell. 2017;169:483–496 e13. [PubMed: 28413068]
82. Pepe-Mooney BJ, Dill MT, Alemany A, Ordovas-Montanes J, Matsushita Y, Rao A, Sen A, Miyazaki M, Anakk S, et al. Single-Cell Analysis of the Liver Epithelium Reveals Dynamic Heterogeneity and an Essential Role for YAP in Homeostasis and Regeneration. Cell Stem Cell. 2019;25:23-38 e8. [PubMed: 31080134]
83. Bassat E, Mutlak YE, Genzelinakh A, Shadrin IY, Baruch Umansky K, Yifa O, Kain D, Rajchman D, Leach J, et al. The extracellular matrix protein agrin promotes heart regeneration in mice. Nature. 2017;547:179–184. [PubMed: 28581497]

CLINICAL PERSPECTIVE

What's New?

1. A subset of epicardial cells emerges in post-embryonic zebrafish, expresses *hapln1* paralogs, and surrounds regions of active cardiomyogenesis in contexts of heart morphogenesis and injury-induced regeneration.
2. Induced genetic depletion of *hapln1a*-expressing cells or genetic inactivation of *hapln1b* disrupts cardiomyocyte proliferation and inhibits heart regeneration.
3. *hapln1*-expressing cells or activity is required to produce a matrix rich with organized HA in injury sites.

What Are the Clinical Implications?

1. Targeting HA regulation by manipulation of HAPLN1 in human epicardial cells could potentially modulate cardiac repair after myocardial infarction.
2. Matrix regulation by subsets of epicardial cells might also be key for localized cardiomyocyte proliferation during human heart development, which would be relevant to understanding the basis of congenital cardiac disease.

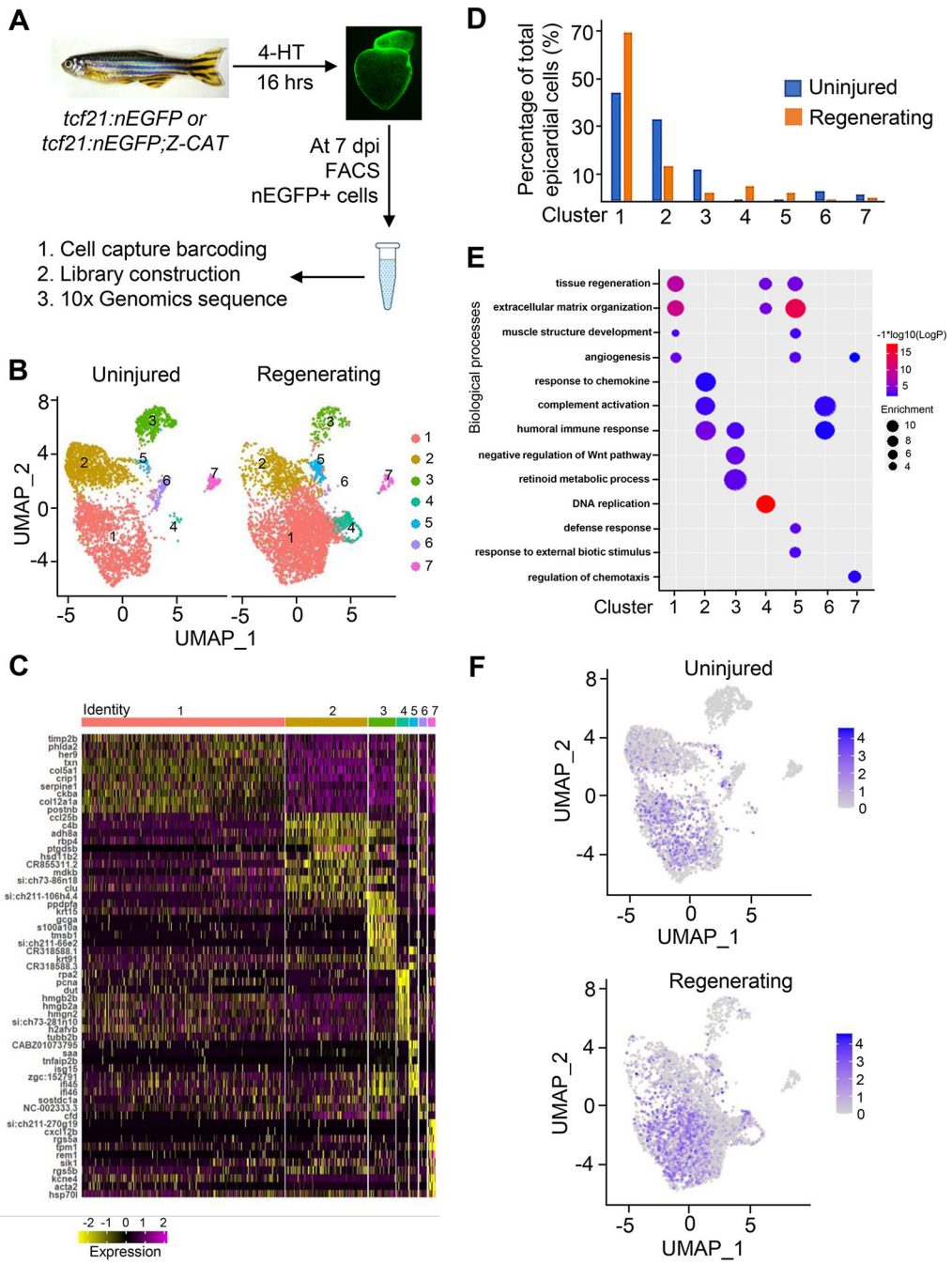

Figure 1. Single-cell RNA-sequencing reveals distinct epicardial cell clusters in zebrafish during heart regeneration.

(A) Schematic representation of the scRNA-seq workflow. Z-CAT: zebrafish cardiomyocyte ablation transgenes (*cmlc2:CreER*;*bactin2:loxp-mCherry-STOP-loxp-DTA*). One hundred *tcf21:nEGFP* and 70 *tcf21:nEGFP;Z-CAT* were used.

(B) Uniform manifold approximation and projection (UMAP) clustering of single-cell samples.

(C) Heatmap of the top 10 markers for the epicardial cells from *tcf21:nucEGFP; Z-CAT* animals at 7 days post 4-HT treatment.

(D) Cell clusters as a percentage of epicardial cells in uninjured and regenerating hearts.
(E) Identification of cell clusters based on marker gene expression.
(F) Feature plot of *hapln1a* expression in epicardial clusters of uninjured and regenerating hearts. There are 787 *hapln1a*$^{+}$ cells from uninjured hearts and 1702 *hapln1a*$^{+}$ cells from regenerating hearts.

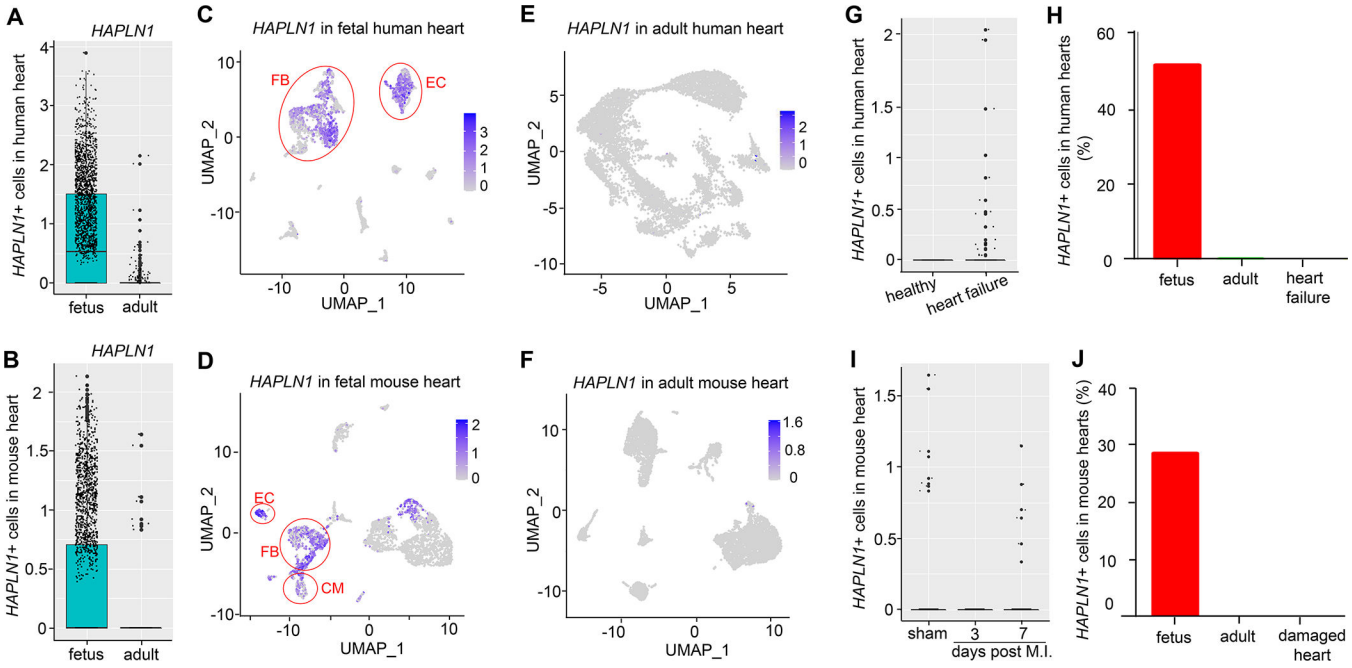

Figure 2. *HAPLN1* expression in mammalian fetal, adult and damaged hearts, assessed by re-analyzing published scRNA-seq datasets.

(A, B) Box plots comparing cardiac cells with *HAPLN1* expression in fetal and adult human hearts (A), and fetal and adult mouse hearts (B).

(C, D) UMAP plot indicating the clusters with *HAPLN*$^{+}$ cells in fetal human (C) and mouse (D) hearts based on the expression of *HAPLN1*. FB, fibroblast; EC, endothelial cells; CM, cardiomyocytes.

(E, F) UMAP plot indicating the clusters with *HAPLN1*$^{+}$ cells in adult human (E) and mouse (F) hearts based on the expression of *HAPLN1*.

(G) Box plots comparing cardiac cells with *HAPLN1* expression in adult human healthy and failure hearts.

(H) Quantification of *HAPLN1*$^{+}$ cells in fetal, adult, and failure human hearts in (G).

(I) Box plots comparing cardiac cells with mice *HAPLN1* expression in sham control, and myocardial-infarction (MI)- injured mouse hearts by 3 and 7 days post damage.

(J) Quantification of *HAPLN1*$^{+}$ cells in fetal, adult, and damaged mouse hearts in (I).

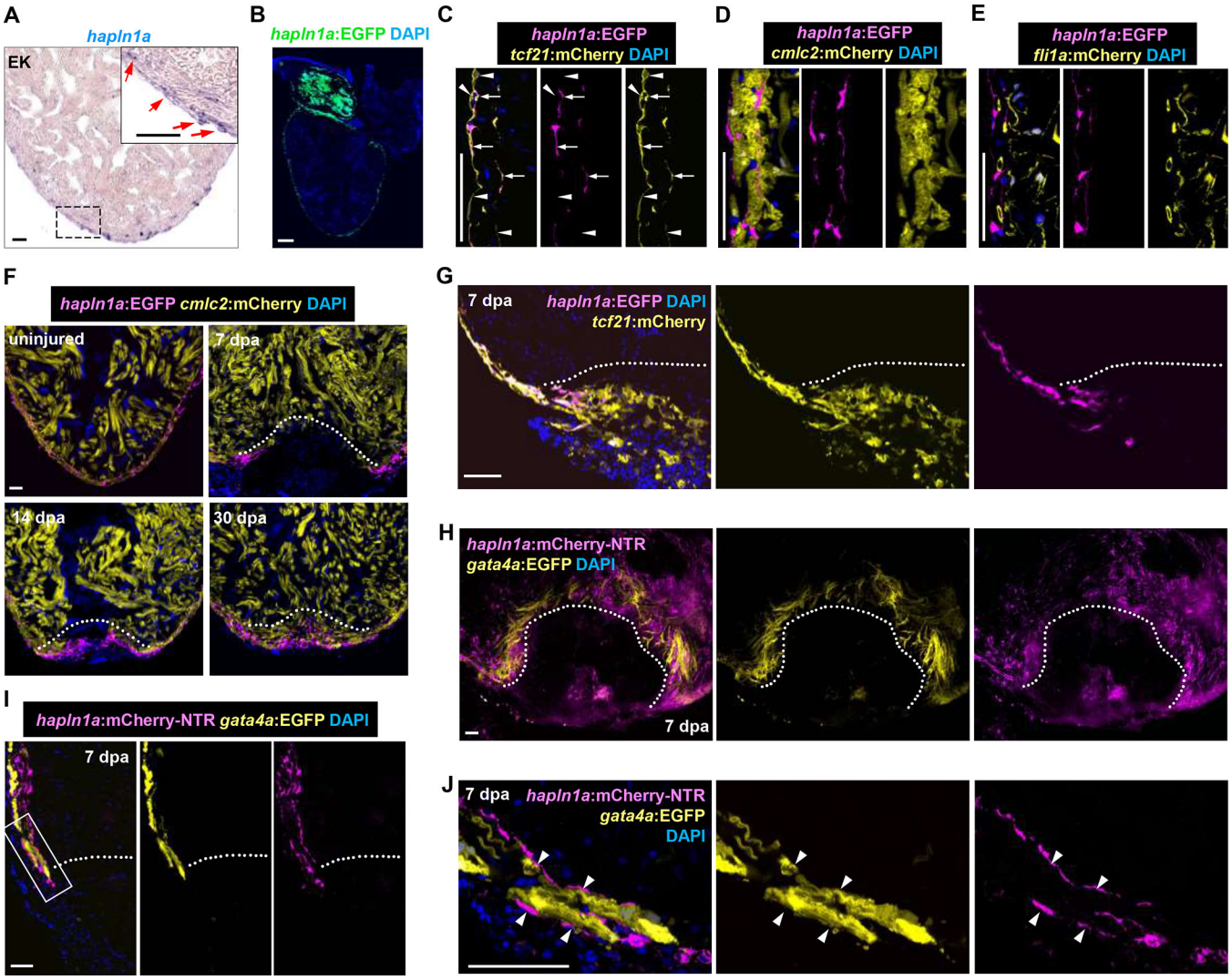

Figure 3. *hapln1a* labels an epicardial subpopulation that is associated with proliferating cardiomyocytes.

(A) *In situ* of *hapln1a* mRNA in a section of an uninjured heart. White arrows indicate *in situ* signals. n = 8. Scale bar, 50 μm.

(B) *hapln1a*$^{+}$ cells visualized in whole cardiac sections from adult *hapln1a:EGFP* animals. Signals are present in epicardium and smooth muscle of the outflow tract. n = 9. Scale bar, 50 μm.

(C) Confocal slices indicating *hapln1a*$^{+}$ cells in uninjured *hapln1a:EGFP;tcf21:mCherry* ventricles. White arrows represent *hapln1a*$^{+}$/*tcf21*$^{+}$ cells, and arrowheads represent *hapln1a*$^{-}$/*tcf21*$^{+}$ cells. n = 8. Scale bar, 50 μm.

(D, E) Confocal slices indicating *hapln1a*$^{+}$ cells in adult *hapln1a:EGFP;cmlc2:mCherry* (D) and *hapln1a:EGFP;fli1a:mCherry* (E) ventricles. n = 6–10 in each group. Scale bars, 50 μm.

(F) Visualization of *hapln1a*$^{+}$ cells in *hapln1a:EGFP;cmlc2:mCherry* ventricles without injury and during regeneration at 7, 14 and 30 dpa. Dashed line indicates amputation plane. n = 9 to 12 animals for each timepoint. Scale bars, 50 μm.

(G) Section images of *hapln1a:EGFP;tcf21:mCherry* ventricles during regeneration at 7 dpa, assessed for *hapln1a*$^+$ cells and *tcf21*$^+$ cells in the injury site. These images display a colocalization of EGFP$^+$ signals with a portion of mCherry$^+$ signals in the injury site, with EGFP$^+$/mCherry$^+$ cells comprising 21.23% of the total mCherry$^+$ cells in the injury site. Dashed line indicates amputation plane. n = 10. Scale bar, 50 μm.

(H) Whole-mount view of *hapln1a*$^+$ cells and *gata4*:EGFP$^+$ CMs in the injured area of *hapln1a:mCherry-NTR;gata4:EGFP* fish hearts at 7 dpa. Dashed line indicates amputation plane. n = 12. Scale bar, 50 μm.

(I, J) Section images of *hapln1a:mCherry-NTR;gata4:EGFP* ventricles at 7 dpa, assessed for *hapln1a*$^+$ cells and *gata4*:EGFP$^+$ CMs in the injury site. The box area in (I) is shown in higher magnification in (J). Arrowheads represent *hapln1a*$^+$ cells lining and surrounding *gata4*:EGFP$^+$ CMs. Dashed line indicates amputation plane. n = 15. Scale bar, 50 μm.

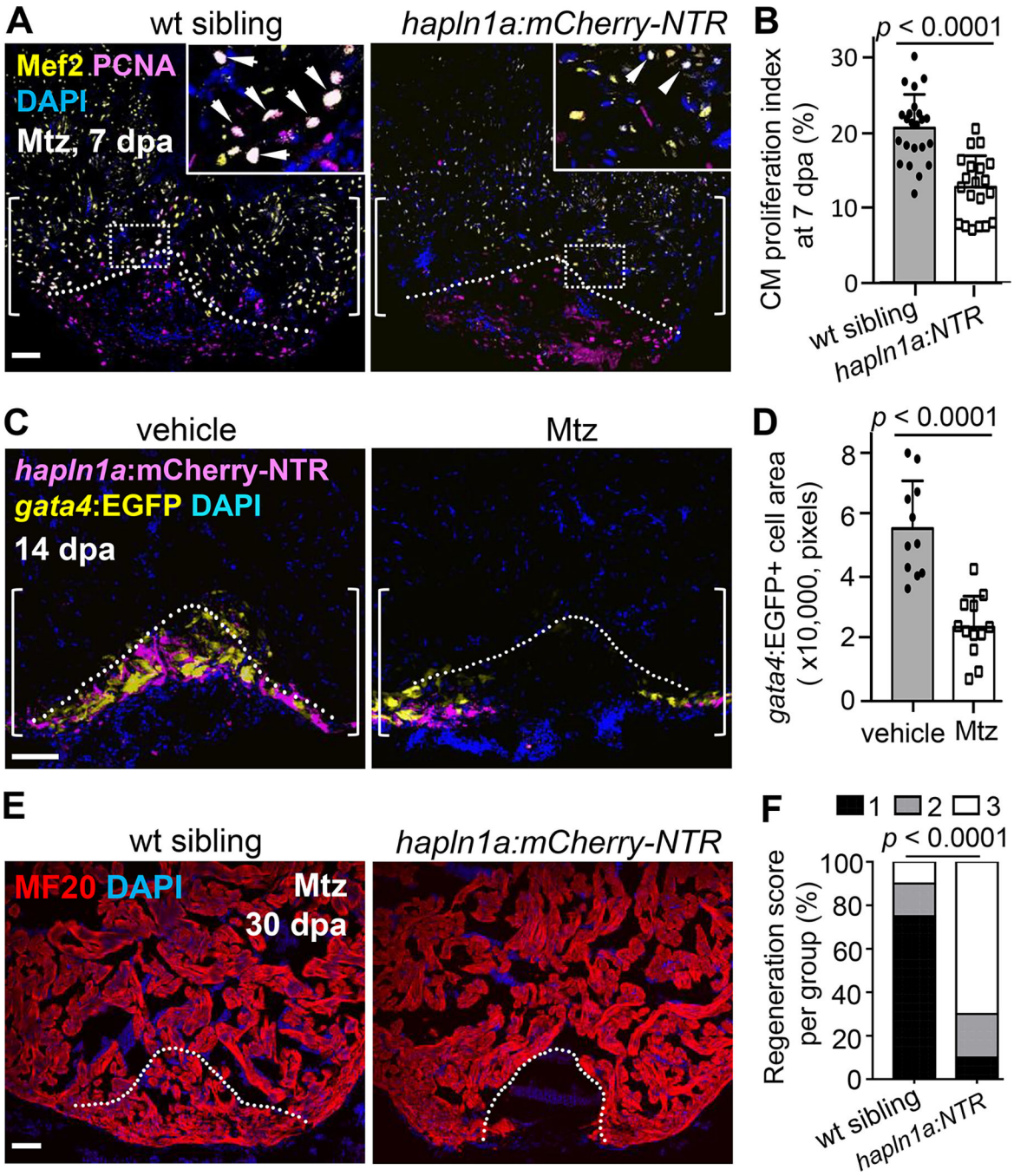

Figure 4. *hapln1a*$^{+}$ cells are required for myocardial regeneration.

(A) CM proliferation in ventricular sections from Mtz-treated wild-type siblings and *hapln1a:mCherry-NTR* animals at 7 dpa. Arrowheads represent proliferating Mef2^{+}PCNA^{+} CMs. Brackets, injury site used for quantification. Dashed line indicates amputation plane. Scale bar, 50 μm.

(B) Quantification of CM proliferation in injury sites in experiments from (A). A total of 23 wild-type siblings and 20 *hapln1a:mCherry-NTR* fish hearts were assessed from two experiments. Mann-Whitney Rank Sum test.

(C) Section images of ventricles of vehicle- or Mtz-treated *hapln1a:mCherry-NTR;gata4:EGFP* at 14 dpa, assessed for *gata4*:EGFP$^+$ CMs in the injury site. Brackets, injury site used for quantification. Dashed line indicates amputation plane. Scale bars, 50 μm.

(D) Quantification of EGFP$^+$ pixels in cardiac wounds from experiments in (C). A total of 21 vehicle-treated and 25 Mtz-treated *hapln1a:mCherry-NTR* fish hearts were assessed from two experiments. Mann-Whitney Rank Sum test.

(E, F) Section images (E) of Mtz-treated wild-type siblings or *hapln1a:mCherry-NTR* ventricles at 30 dpa assessed for muscle recovery, and quantification of regeneration indices (F). A total of 20 *hapln1a*$^+$ cell-depleted animals and 20 control siblings was examined from two experiments. Myocardial regeneration is categorized as: 1, complete regeneration of a new myocardial wall; 2, partial regeneration; and 3, a strong block in regeneration. Five of 20 control siblings and 18 of 20 *hapln1a*$^+$ cell-depleted ventricles showed prominent myocardial gaps. Chi-squared test. Dashed line indicates amputation plane. Scale bar, 50 μm.

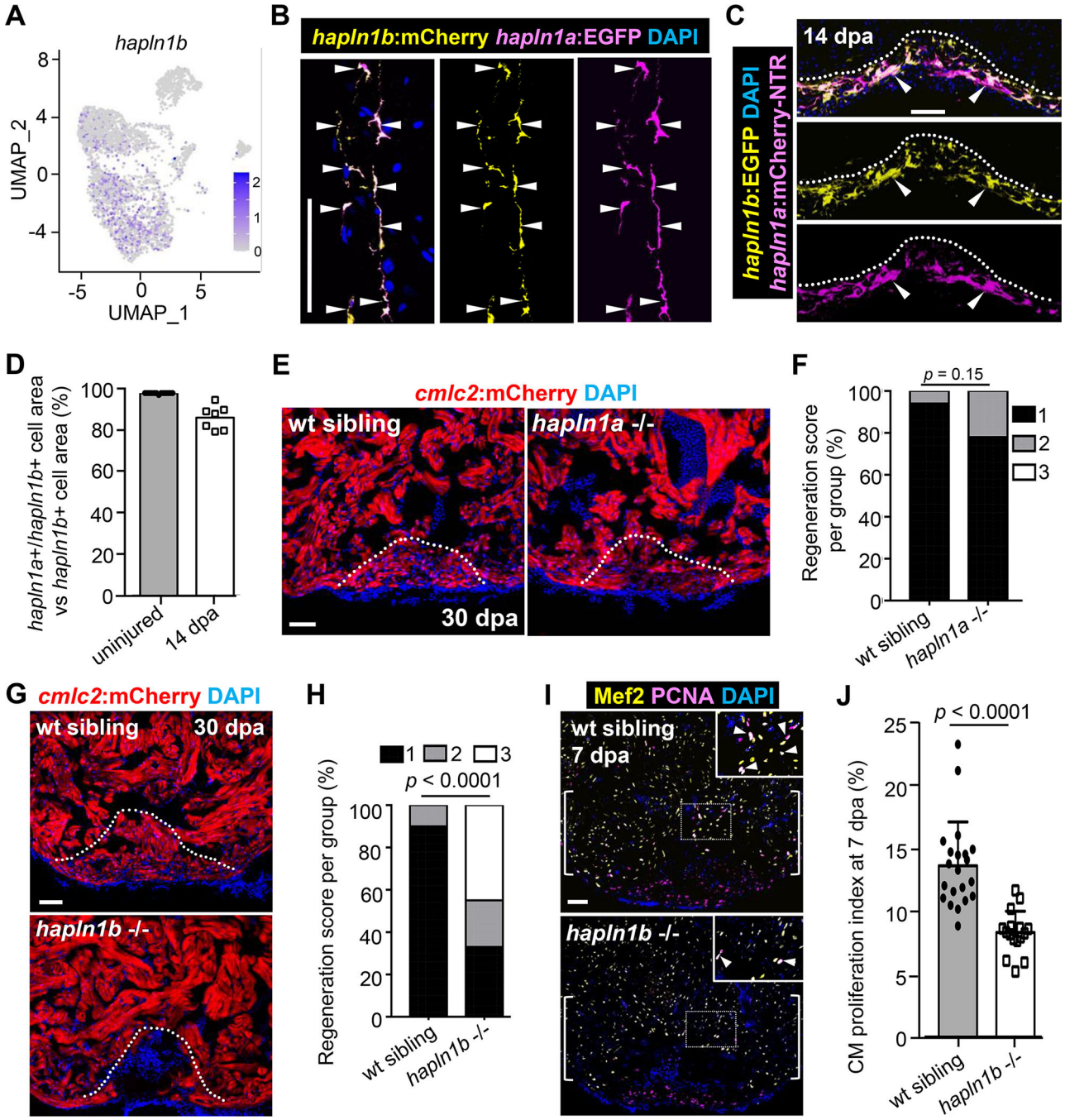

Figure 5. Hapln1b is required for injury-induced cardiomyocyte proliferation and heart regeneration.

(A) Feature plot of *hapln1b* expression in epicardial clusters from uninjured heart samples.

(B) Visualization of *hapln1a*$^{+}$ and *hapln1b*$^{+}$ cells in ventricular sections from uninjured adult *hapln1a:EGFP;hapn1b:mCherry* animals. Arrowheads represent *hapln1a*$^{+}$/*hapln1b*$^{+}$ cells. n = 11. Scale bar, 50 μm.

(C) Visualization of *hapln1a*$^{+}$ and *hapln1b*$^{+}$ cells in injury sites in ventricular sections from adult *hapln1a:mCherry-NTR;hapn1b:EGFP* animals at 14 dpa. White dashed lines indicate

the amputation plane. Arrowheads represent *hapln1a*+/*hapln1b*+ cells. n = 7. Scale bar, 50 μm.

(D) Quantification of *hapln1a*$^{+}$ cells as a percentage of total *hapln1b*$^{+}$ cells in experiments from (B) and (C), based on areas of fluorescence. Mann-Whitney Rank Sum test. Scale bar, 50 μm.

(E, F) Section images (E) and quantification (F) of *hapln1a* mutant and wild-type sibling ventricles, assessed for muscle recovery at 30 dpa. A total of 23 *hapln1a* mutant animals and 18 wild-type siblings were assessed from two experiments. One of 18 wild-type siblings and 5 of 23 *hapln1a* mutants showed partial myocardial regeneration. Chi-squared test. Dashed line indicates amputation plane. Scale bar, 50 μm.

(G, H) Section images (G) and quantified regeneration indices (H) of injured *hapln1b* mutant and wild-type sibling ventricles, assessed for muscle recovery at 30 dpa. A total of 22 *hapln1b* mutant animals and 21 wild-type siblings were assessed from two experiments. Zero of 21 wild-type siblings and 18 of 22 *hapln1b* mutants displayed prominent myocardial gaps. Chi-squared test. Dashed line indicates amputation plane. Scale bar, 50 μm.

(I) Cardiomyocyte (CM) proliferation in *hapln1b* mutant and wild-type sibling hearts at 7 dpa, stained with antibodies against Mef2 for CM nuclei and PCNA. Arrowheads represent proliferating CMs. Brackets, injury site used for quantification. Scale bar, 50 μm.

(J) Quantification of CM proliferation in injury sites in experiments from (I). A total of 16 *hapln1b* mutant animals and 21 wild-type siblings were assessed from two experiments. Mann-Whitney Rank Sum test.

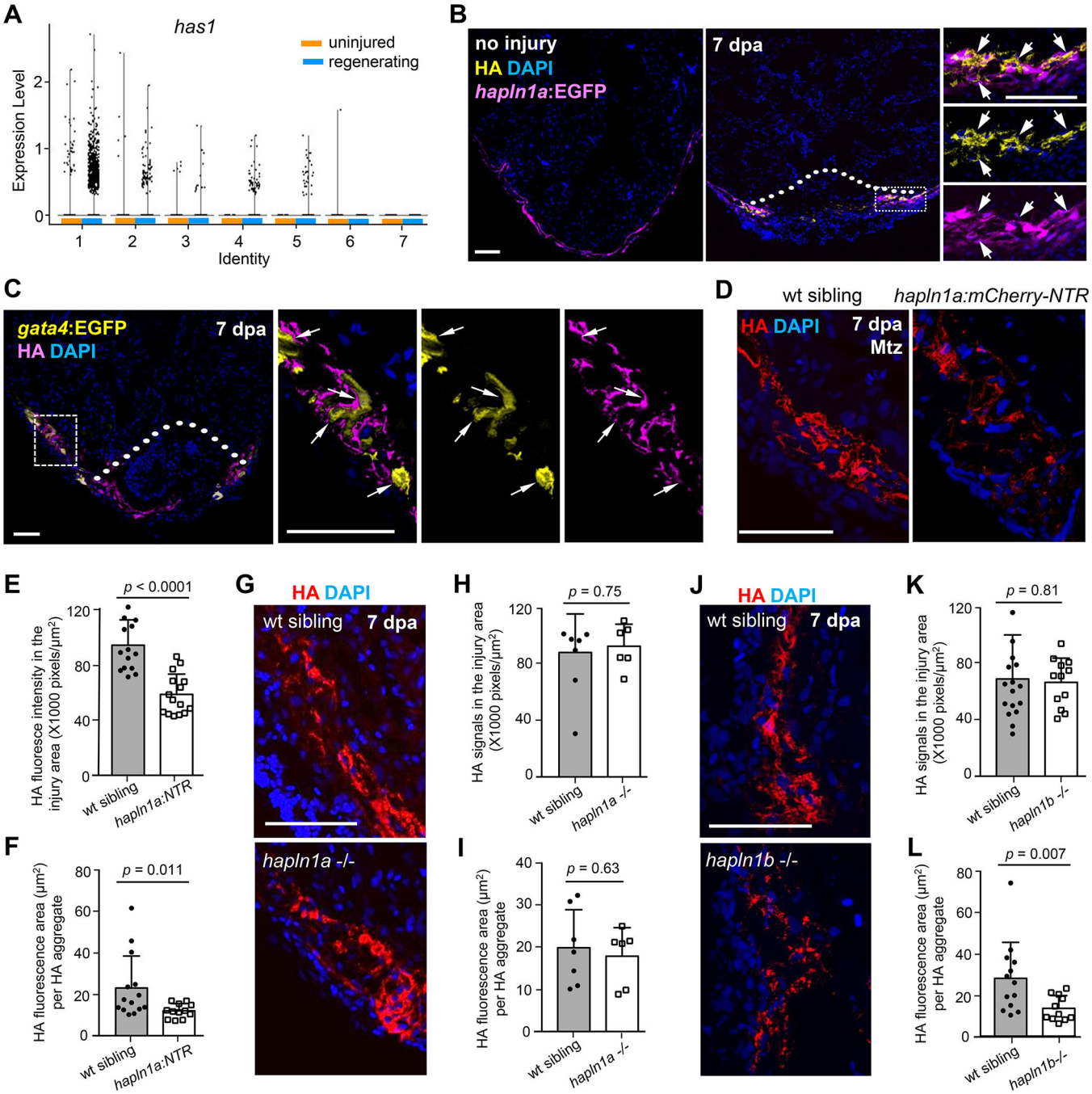

Fig. 6. Depletion of *hapln1a*$^+$ cells or inactivation of *hapln1b* results in defective hyaluronic acid deposition in regenerating hearts.

(A) Violin-plot of *has1* expression in *tcf21*$^+$ epicardial cell clusters in uninjured and regenerating hearts.

(B) Section images of *hapln1a:EGFP* ventricles without injury and at 7 dpa, assessed for *hapln1a*$^+$ cells and HA signals in the injury site. The boxed area was visualized with high magnification. Arrows represent *hapln1a*$^+$ cells lining with HA signals. n = 8. Dashed line indicates amputation plane. Scale bar, 50 μm.

(C) Section images of *gata4:EGFP* ventricles at 7 dpa, assessed for *gata4*:EGFP$^+$ cells and HA signals in the injury site. The boxed area was visualized with high magnification. Arrowheads represent *gata4*:EGFP$^+$ cells lining and surrounding with HA signals. n = 7. Scale bar, 50 μm.

(D) Section images of ventricles of *hapln1a:mCherry-NTR* or control siblings with Mtz treatment at 7 dpa, assessed for HA signals in the injury site. Scale bar, 50 μm.

(E, F) Quantification of HA$^+$ fluorescence pixels (E) and HA signals per area (F) in injury edges from experiments in (D). A total of 15 *hapln1a:mCherry-NTR* and 15 control sibling hearts were assessed from two experiments. Mann-Whitney Rank Sum test.

(G) Section images of ventricles of *hapln1a* −/− and wild-type siblings at 7dpa, assessed for HA signals in the injury site. Scale bar, 50 μm.

(H, I) Quantification of HA$^+$ fluorescence pixels (H) and HA signal area per HA aggregate (I) in the injury edges from experiments in (G). Eleven *hapln1a* −/− and 13 wild-type siblings were analyzed. Mann-Whitney Rank Sum test.

(J) Section images of ventricles of *hapln1b* −/− and wild-type siblings at 7dpa, assessed for HA signals in the injury site. Scale bar, 50 μm.

(K, L) Quantification of HA$^+$ fluorescence pixels (K) and HA signal area per HA aggregate (L) in the injury edges from experiments in (J). Total twelve *hapln1b* −/− and 16 wild-type siblings were analyzed from two experiments. Mann-Whitney Rank Sum test.

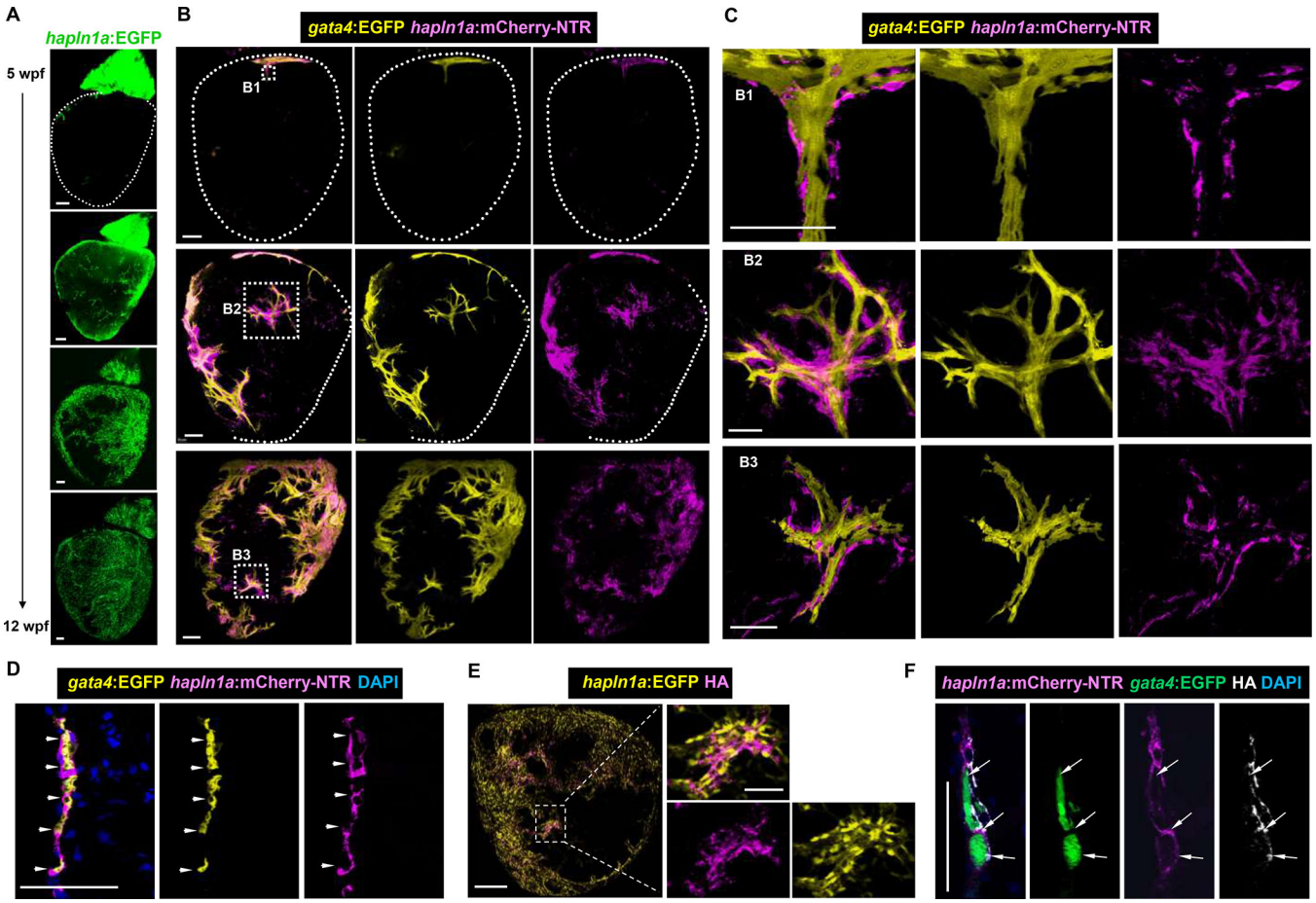

Figure 7. *hapln1a*$^{+}$ cells associate with emergent *gata4*:EGFP^{+} cardiomyocytes and HA in juvenile ventricles.

(A) Whole-mount views of *hapln1a*$^{+}$ cells on the *hapln1a:EGFP* ventricular surface (opposite the atrioventricular junction) from 5 to 12 weeks post fertilization. Dashed lines indicate ventricular periphery. n = 10–20 animals for each timepoint. Scale bars, 100 μm.

(B) Whole-mount visualization of *hapln1a*$^{+}$ cells and *gata4*:EGFP^{+} CMs on the *hapln1a:mCherry;gata4:EGFP* ventricular surface (opposite the atrioventricular junction) from 5 to 12 weeks post fertilization. A total of 50 juvenile animals were assessed. Scale bars, 100 μm.

(C) Magenta areas (B1, B2, and B3) in (B) were enlarged, highlighting close juxtaposition of *gata4*$^{+}$ and *hapln1a*$^{+}$ cells. Scale bars, 50 μm.

(D) Visualization of *hapln1a*$^{+}$ cells and *gata4*:EGFP^{+} CMs in sections of juvenile *hapln1a:mCherry;gata4:EGFP* ventricles. Ten animals were assessed. Scale bars, 50 μm.

(E) *hapln1a*$^{+}$ cells and hyaluronan acid (HA) fluorescence signals visualized in whole-mount view of the ventricles of juvenile *hapln1a:EGFP* animals at the age of 2 months post fertilization (mpf), assessed by HA staining. HA signals are present in *hapln1a*$^{+}$ cell-distributed area. The boxed area is enlarged. n = 11. Scale bars, 100 μm.

(F) Section views of *gata4*:EGFP^{+} CMs, *hapln1a*$^{+}$ cells and HA fluorescence signals from ventricles of juvenile *gata4:EGFP;hapln1a:mCherry-NTR* animals, assessed by HA

fluorescence staining. Arrows indicate *gata4*:EGFP^{+} CMs lining with *hapln1a*$^{+}$ cells and HA^{+} fluorescence signals. n = 7. Scale bar, 50 μm.

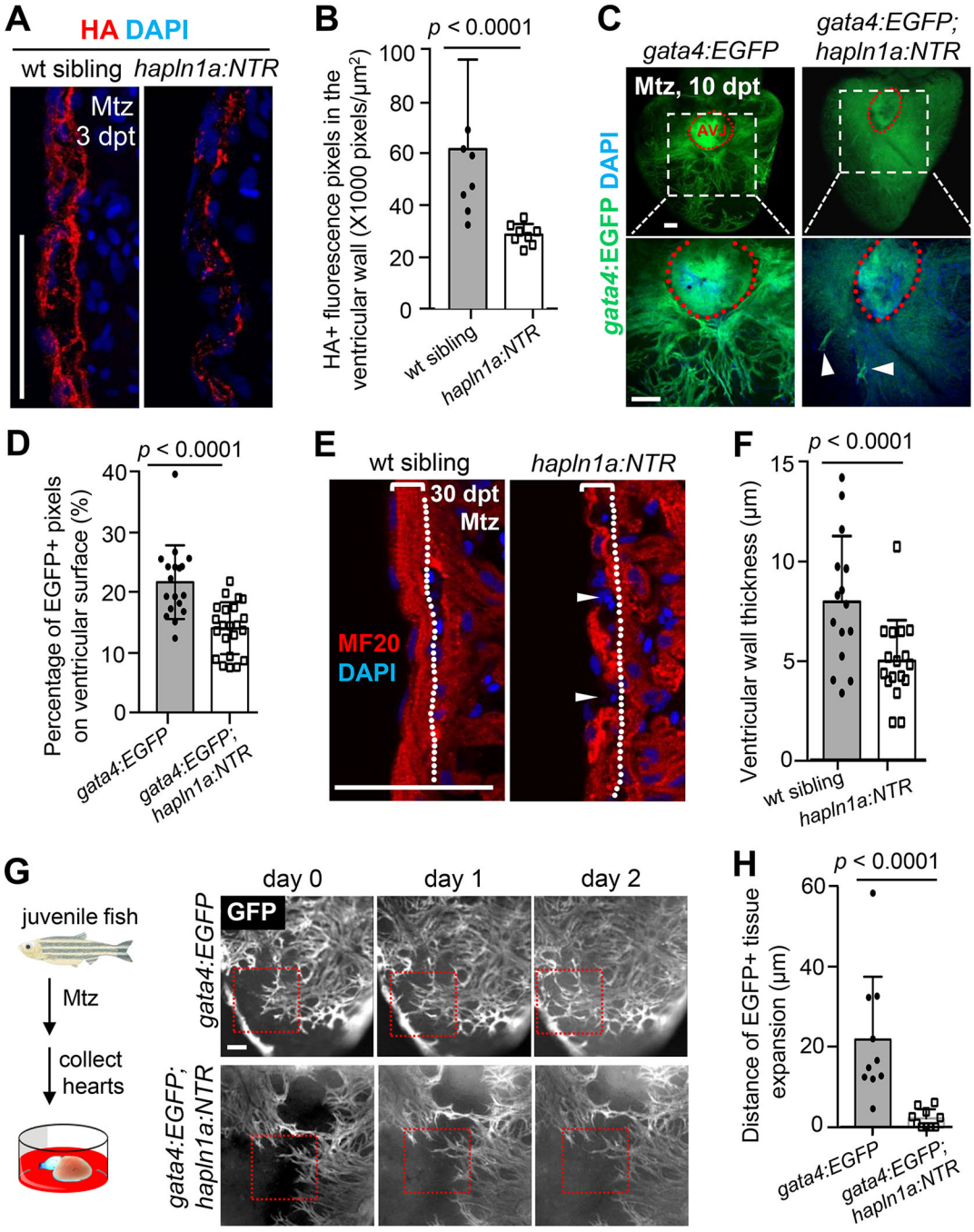

Figure 8. *hapln1a*$^{+}$ cells are required for morphogenesis of the compact myocardium.

(A) Section images of the ventricles of Mtz-treated juvenile *hapln1a:mCherry-NTR* or wild-type siblings at 3 days post Mtz-treatment (dpt), assessed for HA antibody staining in the ventricular wall. Scale bar, 50 μm.

(B) Quantification of HA^{+} fluorescence pixels in the ventricular wall from experiments in (A). A total of 8 Mtz-treated *hapln1a:mCherry-NTR* fish and 8 control sibling hearts were assessed from two experiments. Mann-Whitney Rank Sum test.

(C) Visualization of *gata4*$^{+}$ cardiomyocytes in whole-mounted juvenile *gata4:EGFP* and *gata4:EGFP;hapln1a:mCherry-NTR* hearts after Mtz treatment. Boxed area is enlarged with high magnification in the panels below. Arrowheads represent EGFP signals in *hapln1a* cell-depleted hearts. AVJ, Atrium-ventricle junction. n = 18–20, in each group. Scale bars, 50 μm.

(D) Quantification of the percentage of EGFP^{+} pixels on the ventricular surface from experiments in (C). Mann-Whitney Rank Sum test.

(E) Section view of the compact muscle layer in *hapln1a:mCherry-NTR* and wild-type ventricles 30 days after Mtz treatment. Arrowheads represent discontinuities in the cortical wall in *hapln1a* cell-depleted hearts. 16–18 animals were assessed for each group and repeated once. Dashed line represents the boundary separating ventricular wall and the inner ventricle. Scale bar, 50 μm.

(F) Quantification of ventricular wall thickness in (E). Mann-Whitney Rank Sum test.

(G) (Left) Schematic to visualize cardiomyocyte growth in control and *hapln1a*$^{+}$ cell-depleted juvenile hearts *ex vivo*. (Right) Visualization of *gata4*:EGFP^{+} tissue growth in juvenile *gata4:EGFP* and *gata4:EGFP;hapln1a:mCherry-NTR* hearts over 2 days after Mtz treatment. *gata4*:EGFP^{+} tissue growth is clear in *gata4:EGFP* ventricles (top; n = 11 out of 11); growth of this extent is rarely observed in *hapln1a:NTR;gata4:EGFP* ventricles (bottom; n = 2 out of 13). Red boxes represent *gata4*:EGFP^{+} cardiac muscle expansion. Chi-square test. Scale bar, 300 μm.

(H) Quantification of distances of *gata4*:EGFP^{+} tissue expansion over two days, from experiments in (G). Mann-Whitney Rank Sum test.